Effects of deposition time and post-deposition annealing on the physical and chemical properties of electrodeposited CdS thin films for solar cell application

ECHEND, O.K., MBAMARA, U.S., OKEOMA, K.B., IROEGBU, C., MADU, C. A., NDUKWE, I.C. and DHARMADASA, I.M. <http://orcid.org/0000-0001-7988-669X>

Effects of deposition time and post-deposition annealing on the physical and chemical properties of electrodeposited CdS thin films for solar cell application

O. K. Echendu[*1,2], U. S. Mbamara[2], K. B. Okeoma[2], C. Iroegbu[2], C. A. Madu[2], , I. C. Ndukwe[2] and I. M. Dharmadasa[1]

[1]Electronic Materials and Sensors Group, Materials and Engineering Research Institute,

Sheffield Hallam University, S1 1WB, Sheffield, UK.

[2]Thin Film Research Group, Department of Physics, Federal University of Technology,

P. M. B. 1526, Owerri, Nigeria.

*Corresponding author's email: oechendu@yahoo.com

Abstract

CdS thin films were cathodically electrodeposited by means of a two-electrode deposition system for different durations. The films were characterised for their structural, optical, morphological and compositional properties using x-ray diffraction (XRD), spectrophotometry, scanning electron microscopy (SEM) and energy dispersive x-ray (EDX) respectively. The results obtained show that the physical and chemical properties of these films are significantly influenced by the deposition time and post-deposition annealing. This influence manifests more in the as-deposited materials than in the annealed ones. XRD results show that the crystallite sizes of the different films are in the range (9.4 – 65.8) nm and (16.4 – 66.0) nm in the as-deposited and annealed forms respectively. Optical measurements show that the absorption coefficients are in the range $(2.7\times10^4 – 6.7\times10^4)$ cm^{-1} and $(4.3\times10^4 – 7.2\times10^4)$ cm^{-1} respectively for as-deposited and annealed films. The refractive index is in the range (2.40 – 2.60) for as-deposited films and come to the value of 2.37 after annealing. The extinction coefficient varies in the range (0.1 – 0.3) in as-deposited films and becomes 0.1 in annealed films. The estimated energy bandgap of the films is in the range (2.48 – 2.50) eV for as-deposited films and becomes 2.42 eV for all annealed films. EDX results show that all the films are S-rich in chemical composition with fairly uniform Cd/S ratio after annealing. The results show that annealing improves the qualities of the films and deposition time can be used to control the film thickness.

Keywords: Electrodeposition; two-electrode system; CdS; annealing; deposition time; thin-film.

Acknowledgement

The authors thank F. Fauzi, A. N. Abdul-Manaf, M. L. Madugu, I. O. Olusola and A. Ojo for valuable discussions. The principal author wishes to thank the Tertiary Education Trust Fund TETFUND), Nigeria and the Federal University of Technology, Owerri, Nigeria for financial support.

1.0 Introduction

CdS is a wide bandgap semiconductor with a direct bulk bandgap value of 2.42 eV [1]. It has desirable qualities that make it find use in applications such as solar cells (where it is used as a window or buffer material) [2, 3, 4], photoresistors, phosphors, electroluminescence [5], diodes [6], thin film transistors [7] and radiation detectors [8].

To produce CdS, different techniques have been used by different researchers. These include chemical bath deposition (CBD) [9], vacuum evaporation [10] chemical vapour deposition [11], spray pyrolysis [12], sputtering [13], screen printing [14], sol-gel [15], close space sublimation [16] and electrodeposition [17 - 20]. The electrodeposition of CdS has always been reported in the past based on the conventional three-electrode configuration [21] as is common in the electrodeposition of semiconductors. In recent times however, only a few reports on the use of two-electrode system for the electrodeposition of CdS can be found in the literature [17, 20, 22]. Two major reasons for the use of two-electrode system in the electrodeposition of semiconductors include: (i) to prevent any possible contamination of the deposition electrolyte by ions such as Ag^+ and K^+ which may eventually leak into the deposition electrolyte from the commonly used Ag/AgCl and Hg/HgCl (saturated calomel) reference electrodes during the electrodeposition process especially as the reference electrode ages; (ii) to simplify the electrodeposition process and therefore reduce cost.

For CdS/CdTe solar cell fabrication, for example, the CBD process has commonly been used to grow CdS thin films [23 - 25] while CdTe is deposited using CSS [23 - 25], sputtering [13] or electrodeposition [26, 27]. Due to the nature of CBD as a batch process, a lot of Cd-containing waste is generated in the large-scale deposition of CdS. This raises serious environmental concern as well as costs huge sums of money in order to manage and dispose of the waste. This situation poses a problem in a production line, coupled with the use of at least two different deposition techniques. This eventually results in the production of expensive solar panels. In such an industrial process, it is preferable to have only one production line by using only one technique to deposit both CdS and CdTe. A continuous process such as electrodeposition fits into this picture for the production of less expensive solar panels. Based on these reasons, the electrodeposition of CdS thin-films using two-electrode system has been undertaken and reported in this work for possible application in development of all-electrodeposited CdS/CdTe solar cells and other CdS-based devices.

The relevant equations used for deducing the optical parameters (from transmittance and absorbance measurements) of the CdS films are given in (1) – (8) as reported previously [28] below. It is well-known that when light is incident on a thin film material, it is either absorbed, transmitted or reflected, and the sum of the fractions of the absorbed, transmitted and reflected light equals unity, so that

$$A + T + R = 1 \quad (1)$$

where A is absorbance, T is transmittance and R is reflectance.

The overall response of the material to the incident light is connected to its refractive index according to equation (2).

$$N = n + iK \quad (2)$$

where N is the refractive index of the material, n is the real part of the refractive index and K is the imaginary part of the refractive index, also known as the extinction coefficient of the material in question.

The reflectance of the material and the real part of the refractive index are connected by equation (3).

$$R = \frac{(n-1)^2}{(n+1)^2} \quad (3)$$

The absorption coefficient α, of the material is also related to the extinction coefficient according to equation (4).

$$\alpha = \frac{4\pi K}{\lambda} \quad (4)$$

The complex dielectric constant ε, is related to n and K according to equation (5).

$$\varepsilon = (n + iK)^2 = \varepsilon_r + \varepsilon_i \quad (5)$$

where ε_r and ε_i are the real and imaginary parts of the dielectric constant of the material respectively.

The absorbance of the thin film is related to its transmittance according to equation (6).

$$A = \log_{10}\left(\frac{1}{T}\right) \quad (6)$$

The absorption coefficient is also related to the transmittance by

$$\alpha = -\ln\left(\frac{T}{d}\right) \quad (7)$$

where d is the thickness of the film.

Finally, for a direct bandgap semiconductor, such as CdS, the absorption coefficient is related to the energy hv, of the absorbed photons and the bandgap energy E_g, of the semiconductor by

$$\alpha = \frac{C\left(hv - E_g\right)^{1/2}}{hv} \qquad (8)$$

Where C is a constant, h is Planck's constant and v is the frequency of the incident photons.

2.0 Experimental procedure

2.1 Preparation of CdS deposition electrolyte

The CdS deposition electrolyte is made up of 0.3 M $CdCl_2.H_2O$ and 0.03 M $Na_2S_2O_3.5H_2O$ in 800 ml of de-ionised water. Both chemicals are laboratory reagent grade purchased from Fisher Scientific, United Kingdom. Before the addition of $Na_2S_2O_3.5H_2O$, the solution containing only $CdCl_2.H_2O$ was stirred for 24 hours to ensure proper dissolution of the $CdCl_2.H_2O$ crystals. The pH of the solution was then adjusted to 1.80±0.02 by adding some drops of dilute HCl. Afterwards, the $CdCl_2.H_2O$ solution was heated to a temperature of (80±2)ºC with stirring at 400 rotations per minute (r.p.m.). A cyclic voltammetry of the electrolyte was then taken using a computerised Gill AC potentiostat (ACM Instruments, Cumbria, UK) in two-electrode configuration, with a clean fluorine-doped tin oxide-coated glass (glass/FTO) as the working electrode and a high-purity carbon rod as the counter electrode. This was done in order to identify the deposition potential of Cd which has a standard reduction potential of -403 mV. From the result of the cyclic voltammetry, the $CdCl_2.H_2O$ electrolyte was electro-purified for 48 hours at a cathodic potential slightly lower than the deposition potential of Cd. This is usually done to get rid of possible ionic impurities present in the $CdCl_2.H_2O$ considering also the higher concentration of $CdCl_2.H_2O$ relative to $Na_2S_2O_3.5H_2O$.

After electro-purification, the 0.03 M $Na_2S_2O_3.5H_2O$ was added into the purified $CdCl_2.H_2O$ solution and stirred for about 6 hours. The pH of the resulting CdS deposition electrolyte was again adjusted to 1.80±0.02 using dilute HCl and NH_4OH. Another cyclic voltammetry was carried out, this time, to identify the range of possible deposition potentials for CdS. The voltammogram (which is the graph of current density vs. applied cathodic potential) for the CdS deposition electrolyte was then plotted as shown in figure 1 from which the possible cathodic deposition potential of CdS was identified to be in the range (1300 – 1500) mV.

2.2 Substrate preparation and electrodeposition of CdS thin films

The glass/FTO substrates used for both cyclic voltammetry and deposition of CdS thin films were cut from a large plate of dimension 30 cm×30 cm×3.0 mm into smaller sizes of dimension 3.0 cm×2.0 cm×3.0 mm. These were cleaned first with soap solution for 15 minutes in an ultrasonic bath. After rinsing with de-ionised water, they were again cleaned with acetone and methanol in turn while rinsing with de-ionised water in-between. Finally, they were dried in a stream of N_2.

To carry out the electrodeposition of CdS, each small glass/FTO substrate was attached to a carbon plate using insulating PTFE tape, and this served as the working electrode or cathode. The same potentiostat used for cyclic voltammetry in two-electrode configuration was used in depositing CdS onto the substrates. In order to determine the best deposition potential for CdS, some preliminary samples were deposited on glass/FTO at different potentials across the initially identified deposition potential range of 1300 mV – 1500 mV, and characterised using x-ray diffraction (XRD) and spectrophotometry. From this, the best cathodic electrodeposition potential for CdS under the conditions described was identified as 1450 mV.

Five CdS thin films were then carefully deposited on glass/FTO at this potential for different durations of 5 minute, 10 minutes, 15 minutes, 20 minutes and 25 minutes, in order to study the effect of deposition time on the properties of the films. After deposition, each sample was rinsed with de-ionised water, dried in a flow of nitrogen and then cut into two equal parts. One set of these parts was designated 'as-deposited' samples while the other set was treated with $CdCl_2$ by dipping them in a saturated solution of $CdCl_2$ in de-ionised water and drying them in air. Afterwards, they were heat-treated at 400 ºC for 20 minutes in a furnace and allowed to cool in air atmosphere. These were designated 'annealed' samples.

2.3 Characterisation of the deposited CdS thin films

The characterisation of the as-deposited and annealed CdS thin films was done using Philips X'Pert Pro x-ray diffraction system (Philips Analytical, Almelo, Australia) for structural properties, Cary 50 UV-VIS spectrophotometer (Varian, Australia Pty Ltd) for optical properties, FEG NOVA NANO scanning electron microscope (FEI Company, The Netherlands) for morphological properties and energy dispersive x-ray (EDX) using EDX detector (Oxford Instruments, UK) attached to the SEM equipment. Thicknesses of the films were measured using UBM Microfocus optical measuring system (UBM, Messetechnik GmbH, Ettlingen, Germany). The results of the characterisation of these films are presented in the following section.

3.0 Results and discussion

3.1 Effect of deposition time on thickness of electrodeposited CdS thin films

Figure 2 shows the effect of deposition time on the thickness of the five electrodeposited CdS thin film samples. The figure shows that the thickness of deposited CdS layers increases as deposition time increases. This relationship is however not linear. The reason for this nonlinearity is not far-fetched. The condition of the deposition bath at the time of growth of each sample plays a significant role. Experience shows that because of the problem of sulphur precipitation, especially at elevated temperatures like the ones used in this experiment the concentration of sulphur in the deposition electrolyte runs low very easily. This usually manifests in drop in the deposition current density and therefore the deposition rate. To try to restore the concentration of sulphur in the electrolyte, a calculated amount of the sulphur source ($Na_2S_2O_3$)

is usually added to the bath from time to time and the deposition current density is controlled by adjusting the stirring rate. This could explain the fluctuation observed in the thickness of the samples under constant temperature and deposition potential since the manual addition of the S^{2-} source may not be very precise.
The same thing could happen with Cd^{2+} but to bring this situation under control, and as a trick in electrodeposition, the initial concentration of Cd^{2+} is made higher (10 times higher in this case) than that of S^{2-} in the electrolyte. This is one of the reasons why the ratio of the concentration of these two ions in the bath is $[Cd^{2+}] / [S^{2-}] = 10 / 1$.

3.2 Effect of deposition time and annealing on the structural properties of the CdS thin films - X-ray diffraction study

Figures 3 (a) and (b) show the XRD patterns of the five electrodeposited CdS thin films, before and after annealing respectively. Looking at the figures, up to a deposition time of 10 minutes, the XRD features did not show up clearly, suggesting that the material at this early formation stage is either weakly crystalline and/or very thin. From 15 minutes of growth and above, the material begins to crystallise and become thicker, and the XRD peaks begin to show up more clearly. A possible reason for this observed poor crystalline (or rather amorphous) nature of CdS at the initial nucleation and formation stage is the fact that the formation of sulphur atoms starts first at the cathode before the formation of Cd atoms begins. This prior formation of sulphur then helps to drive the deposition of Cd. At the initial stage therefore more sulphur gets deposited on the cathode with only very little amount of Cd. As the deposition progresses in time, more and more Cd is attracted to and deposited on the cathode leading to the formation of CdS with increased Cd-content as the two species react together at the cathode. As a result, CdS peaks begin to show up in the XRD at these elevated growth times.

Table 1 shows the structural parameters of the deposited CdS films extracted from the XRD data. The fact that the deposition of CdS on the substrate is still at the nucleation/formation stage is evident in lack of some structural parameters as shown in Table 1 for the films grown for 5 – 10 minutes. As the deposition time increases, all the structural parameters corresponding to the respective XRD peaks begin to show up clearly. The XRD results shown in figure 3 and Table 1 closely match the standard reference Joint Committee on Powder Diffraction and Standards (JCPDF) file no. 01-075-1545. This file has the 2θ and d-spacing values for the three main XRD peaks of hexagonal CdS as follows: [$2\theta = 24.80^{o}$; d-spacing = 3.587 Å]; [$2\theta = 26.49^{o}$; d-spacing = 3.362 Å]; [$2\theta = 28.17^{o}$; d-spacing = 3.165 Å].

A close look at the data in Table 1 shows that with the exception of the sample grown for 10 minutes, for the same reasons stated above, all samples exhibit an increase in the d-spacing values and a decrease in the 2θ values. This is an indication of the presence of tensile stress on the crystal planes and the crystallites. Based on the three main XRD peaks of the hexagonal CdS, only the samples grown for 15 minutes and 20 minutes show constant crystallite sizes before and

after annealing for two out of the three 2θ angles simultaneously. The optimum deposition time for CdS under the conditions used in the present work could therefore be in the range of 15 – 20 minutes.

Table 1: Structural parameters of the CdS thin films extracted from XRD measurements.

	As-deposited				Annealed			
Growth Time (min)	2θ (º)	d-spacing (Å)	β (º)	D (nm)	2θ (º)	d-spacing (Å)	β (º)	D (nm)
5	- - - 26.24 - - -	- - - 3.397 - - -	- - - 0.1624 - - -	- - - 50.5 - - -	25.14 26.20 - - -	3.543 3.401 - - -	0.5196 0.1624 - - -	16.4 52.6 - - -
10	25.17 26.23 28.07	3.539 3.398 3.179	0.9092 0.1624 0.3247	9.4 52.6 26.4	- - - 26.21 28.00	- - - 3.400 3.287	- - - 0.1624 0.1299	- - - 52.6 66.0
15	24.64 26.24 28.09	3.613 3.397 3,177	0.1948 0.1948 0.1948	43.7 43.9 44.0	24.64 26.23 27.98	3.613 3.398 3.189	0.1948 0.1624 0.1948	43.7 52.6 44.0
20	24.67 26.23 28.08	3.609 3.397 3.178	0.1624 0.1624 0.2598	52.5 52.6 33.0	24.65 26.25 28.03	3.611 3.395 3.183	0.1948 0.1624 0.2598	43.7 52.6 33.0
25	24.62 26.19 28.05	3.616 3.403 3.181	0.1948 0.1299 0.2598	43.7 65.8 33.0	24.55 26.18 27.95	3.626 3.404 3.193	0.1948 0.2273 0.1948	43.7 37.6 44.0

3.3 Effect of deposition time and annealing on the optical properties of CdS thin films – Spectrophotometry study

In this section the results of the effect of growth time and annealing on optical properties of the five electrodeposited CdS thin films under study are presented. Figures 4 (a) and (b) show the absorbance spectra of these samples before and after post-deposition annealing respectively.

Figure 4 (a) shows large scatter in the absorbance of the as-deposited films. The films also show significant absorbance in the long wavelength region with weak absorbance edges. In the annealed samples (fig 4 (b)), the absorbance curves show more defined absorbance edges with reduced spread in absorbance. There is also considerable reduction in the absorption of photons (over 50%) in the long wavelength region of the spectrum especially for the thicker samples. The raised absorption tail in the (for the thicker) as-deposited samples indicates the presence of significant amount of photon scattering in these materials. This may be due to the presence of mixed phases, poor stoichiometry and strain/stress in the samples as was pointed out earlier in the XRD study. After annealing, CdS materials with improved qualities are obtained with

significantly reduced scattering, hence the results in figure 4 (b).

Figures 5 (a) and (b) show the transmittance spectra of the as-deposited and annealed CdS films of different deposition times/thicknesses respectively. In both figures, one observes that transmittance decreases as film thickness increases. Also transmittance increases as incident photon wavelength increases. For films with thicknesses ≥201 nm, there is little or no significant transmission of light in the lower wavelengths up to 480 nm. However, for the thinnest sample with thickness of 127 nm, there is relatively significant transmission of photons in this wavelength range with up to 50% transmittance. This, in addition to the high absorption coefficient of CdS, explains the reason why it has been said by some researchers that for application in solar cells as window material, CdS needs to have very small thickness, even as small as (10 - 50) nm [1]. The problem in this situation however, is the issue of good coverage of the underlying TCO substrate. If the thickness of CdS is too low, it may not properly cover the TCO surface and this leads to short-circuiting when an absorber material such as CdTe is deposited on CdS for solar cell fabrication, for example. However, if the particular CdS used is highly photoactive, then very thin layer is not necessary as absorption of photons by the CdS layer helps to create more photo-generated charge carriers.

A close observation of figures 5 (a) and (b) shows that the transmittance spectra in the as-deposited CdS films show wider spread in the entire wavelength range under consideration compared to those of the annealed films. This also points to the fact that the optical quality of these films is improved by post-deposition annealing, since electrodeposition is a low-temperature deposition technique (usually done at temperatures lower than 100 ºC in aqueous solution) compared to other advanced semiconductor growth techniques.

Figures 6 (a) and (b) show the variation of reflectance with photon wavelength for the as-deposited and annealed CdS thin films respectively. Both figures show that the reflectance, of all the films has a maximum value of 20%. However, the photon wavelength at which this maximum occurs is strongly thickness (and therefore growth time)-dependent, and this dependence is more profound in the as-deposited films. The annealed films have less spread in the wavelength at which reflectance sets in compared to as-deposited films. As the thickness of the layer increases, this reflectance maximum, as well as the onset of reflectance, shifts towards longer wavelengths.
Towards the longer wavelengths from the point of maximum reflectance, the reflectance falls rapidly. This result shows that if a very thin CdS film (thickness in the range ≤ 127 nm) is used as a window layer for example in CdS/CdTe solar cell, there will be significant reflection of the incident photons in the short wavelength regions back into the atmosphere by the thin CdS layer. It is known that photons in this wavelength range cause thermalisation in solar cells as a result of their high energy content. Using very thick CdS layer (thickness in the range > 127 nm) again will result in the reflection of significant amount of photons in the visible region. There should

therefore be a balance somewhere in-between, requiring an optimum thickness of CdS for this kind of application.

Figures 7 (a) and (b) show the graphs of absorption coefficient, α vs. photon energy ($h\nu$) for the as-deposited and annealed CdS thin films respectively. Both figures show similar trend in the dependence of absorption coefficient on incident photon energy. Like in figure 5, the absorption edges are very weak in the as-deposited films (figure 7 (a)), but become sharper after annealing (figure 7 (b)). The spread in the absorption coefficient values is also wider in the as-deposited films compared to the annealed films. Careful observation shows that there is a gradual shift in the absorption coefficient edge of the as-deposited films towards shorter wavelength as film thickness increases, and the absorption coefficient tends to increase with film thickness.
These trends are however not clear in the annealed films as the absorption coefficients of the films tend to close up together, up to the photon energy values where the absorption curve has the highest gradient. From figures 7 (a) and (b), the absorption coefficients of these films in the vicinity of the bandgap energy of CdS (2.42 eV - 2.50 eV) lie in the range (2.7×10^4 – 6.7×10^4) cm^{-1} for as-deposited films and (4.3×10^4 - 7.2×10^4) cm^{-1} for annealed samples. These values are in agreement with literature values for CdS grown by CBD [29, 30].

Figures 8 (a) and (b) show the graphs of $(\alpha h\nu)^2$ vs. photon energy for the as-deposited and annealed CdS films respectively, for the purpose of estimating the energy bandgaps of the films. From figure 8, one observes that the as-deposited CdS films show higher values of $(\alpha h\nu)^2$ than the annealed films. The energy bandgap values estimated from figure 8 (a) for the as-deposited films are in the range (2.48 – 2.50) eV while the bandgaps of the annealed films all come to the same value of ~2.42 eV as seen in figure 8 (b). Around the energy bandgaps, the values of $(\alpha h\nu)^2$ for the as-deposited films roughly increase as film thickness increases, while the trend is not clear for the annealed films.

Figures 9 (a) and (b) show the dependence of extinction coefficient, K on photon energy for the as-deposited and annealed CdS thin films respectively. Figures 9 (a) and (b) follow the trend in absorption coefficient (figure 7), with the as-deposited films displaying higher K-values in the vicinity of the bandgap in the range (0.1 – 0.3) than annealed films whose corresponding K-values come to the value of ~0.1. The extinction coefficient generally increases as photon energy increases for both groups of samples. This shows that incident light will travel farther in the annealed films before getting completely absorbed than in the as-deposited films. Figure 9 (a) shows that K-values roughly increase with film thickness which suggests that incident photons will travel farther in thinner samples before getting completely absorbed.

Figures 10 (a) and (b) show the dependence of refractive index, n with photon energy for the as-deposited and annealed CdS thin films respectively. The refractive index shows maximum values of 2.40 - 2.60 for the as-deposited films and a maximum value of ~2.37 for annealed samples in

the vicinity of the bandgap energy of CdS for all the layers. This shows the improvement and uniformity in the quality of all the films after annealing. In general, as one goes towards higher photon energies, the cut-off value of the refractive index increases as film thickness decreases. The refractive index generally follows a sort of parabolic trend with a maximum. Looking at the annealed films in figure 10 (b), it is seen that below the bandgap energy of the films, the refractive index decreases. Above the bandgap energy, n falls more rapidly. The only exception to this particular trend is the thinnest layer with thickness of 127 nm in which n rather falls very slowly beyond the bandgap energy of CdS. This suggests that there is significant scattering of light of shorter wavelengths in this particular material in line with the observation in the reflectance.

Figures 11 (a) and (b) show the real dielectric constants of the as-deposited and annealed CdS thin films of different thicknesses respectively. The real dielectric constant, ϵ_r has the same feature as the refractive index showing a maximum value of 1.5 – 6.9 for as-deposited films and a value of 6.9 for all the annealed films. The photon energy corresponding to maximum ϵ_r values in each set of films varies slightly according to the thickness of the films; the thicker the film, the lower this energy value. Again, towards lower energy values, from the bandgap energy, the ϵ_r values fall gradually while towards higher energy values, they fall more rapidly. The implication of this behaviour is that these films will exhibit higher capacitive properties in the lower photon energy region than in the higher energy region.

Figures 12 (a) and (b) show the graphs of imaginary dielectric constant, ϵ_i vs. photon energy for as-deposited and annealed CdS thin films respectively. There is no specific trend in the variation of the imaginary dielectric constant with film thickness across the photon energy range under consideration, especially for the as-deposited films. However, the imaginary dielectric constant, ϵ_i in figure 12 (b) decreases as the film thickness increases in the energy region below the bandgap value of the layers. For each layer however, ϵ_i increases with increasing photon energy reaching a maximum value at a certain photon energy beyond which it falls rapidly. This maximum point varies with film thickness slightly towards higher energy as the film thickness decreases. The sample with thickness of 127 nm again displays a different behaviour beyond this maximum energy point. The value of ϵ_i for this layer tends to increase beyond this energy reaching another higher maximum value around photon energy of 3.2 eV.

3.4 Effect of deposition time and annealing on the surface morphology of the CdS thin films - Scanning electron microscopy (SEM) study

Figure 13 shows the SEM images of the five CdS thin films of different thicknesses deposited for different durations. It can be seen that as the thicknesses of the films increase, the grains become clearer and more closely packed. At thicknesses of 127 nm and 201 nm however, the amount of deposited CdS material could not completely cover the FTO substrates. These two samples therefore show significant amount of gaps in-between CdS grains with some FTO grains clearly

exposed as shown. The application of CdS films of these thicknesses, for example, in the fabrication of glass/FTO/CdS/CdTe/metal solar cell or in other electronic devices, using the particular glass/FTO substrates in this work will definitely be a failure as a result of shunting of both CdTe and the metal contact with the FTO which will result in loss of fill factor and open-circuit voltage in solar cells and general poor performance of any other electronic device made with them.

Apart from the 377-nm film (corresponding to a growth time of 20 minutes), the other samples did not show any significant increase in grain size after post-deposition annealing. This suggests that this thickness may be the approximate optimum thickness for CdS based on grain size improvement after annealing for the particular glass/FTO substrates used.

3.5 Effect of deposition time and annealing on the atomic composition of the CdS thin films – EDX study

Table 2 and figure 14 show the percentage S and Cd compositions of the CdS thin films of different thicknesses deposited for different durations in both as-deposited and annealed forms.

Table 2: Percentage S and Cd atomic compositions of CdS films deposited for different durations in both as-deposited and annealed forms.

Vg (mV)	Sample ID	Deposition time (min)	Thickness (nm)	Atomic composition (%)				As-deposited Cd/S	Annealed Cd/S
				As-deposited		Annealed			
				Cd	S	Cd	S		
1450	CS148	5	127	42.2	57.8	39.9	60.1	0.73	0.51
1450	CS147	10	201	44.7	55.3	47.9	52.1	0.81	0.92
1450	CS146	15	295	48.1	51.9	48.8	51.2	0.93	0.95
1450	CS145	20	377	48.6	51.4	48.7	51.3	0.94	0.95
1450	CS144	25	557	48.5	51.5	48.6	51.4	0.94	0.95

The results show generally that as-deposited films are S-rich. As the deposition time (thickness) increases the S content decreases up to the thickness of about 377 nm (20 minutes growth time) and then begins to increase slightly as thickness increases beyond this point. After annealing, all the samples also emerged S-rich. Cd content is observed to decrease for the films grown for 5 minutes relative to its as-deposited form. Nevertheless, for the annealed samples, the Cd content gradually increases with growth time up to 15 minutes before gradually decreasing. The best stoichiometry after annealing comes for growth time in the range (15 - 25) minutes corresponding to thickness in the range (295 - 557) nm according to Table 2 and figure 14 (b). However, the 20 minutes sample (377 nm) and the 25 minutes sample appear to have the best

stoichiometry (Cd/S closest to unity) in both as-deposited and annealed forms.

4 Conclusion

The effects of deposition time and post-deposition annealing on the physical and chemical properties of electrodeposited CdS thin films have been presented. The electrodeposition of these films was carried out using two-electrode system for process simplification and cost reduction. Deposition time was seen to have significant influence on the structural, optical, morphological and chemical composition properties of the deposited CdS films under the conditions described. As the deposition time increased, thickness of the films increased. Increase in deposition time resulted in appearance of more and intense CdS XRD peaks. This also resulted in increased absorbance and reduced transmittance. The optical constants also varied significantly with deposition time/film thickness especially for the as-deposited films, while annealing tends to narrow the spread in these parameters. The morphology of the films showed that there is better coverage of the glass/FTO substrates as deposition time increased and the CdS grains became more compacted. Also, the Cd/S ratio in the as-deposited films gradually increased as deposition time increased while it remained fairly constant after annealing. Post-deposition annealing is generally observed to result in improvement of the physical and chemical properties of the films for all the deposition times/thicknesses considered.

Conflict of interest

The authors declare that they have no conflict of interest.

References

[1] T. M. Razykov, C. S. Ferekides, D. Morel, E. Stefanakos, H. S. Ullal and H. M. Upadhyaya, Solar Energy, 85, 1580 (2011).

[2] A. Bosio, N. Romeo, S. Mazzamuto and V. Canevari, Prog. Cryst. Growth & Charact. Mater., 52, 247 (2006).

[3] O. K. Echendu and I. M. Dharmadasa, Energies, 8, 4416 (2015).

[4] N. Naghavi, G. Renou, V. Bockelee, F. Donsanti, P. Genevee, M. Jubault, J. F. Guillemoles and D. Lincot, Thin Solid Films, 519 (21), 7600 (2011).

[5] Y. Kraftmankher, European Journal of Physics 33, 503 (2012).

[6] S. Guduru, V. P. Singh, S. Rajaputra, S. Mishra, R. Mangu and I. S. Omer, Thin Solid Films, 518, 7, 1809 (2010).

[7] W. Wondmagegn, I. Meiia, A. Salas-Villasenor, H. J. Stiegler, M. A. Quevedo-Lopez, R. J. Pieper and B. E. Gnade, Microelectronic Engineering, 157, 64 (2016).

[8] M. R. Balboul, A. Abdel-Galil, I. S. Yahia and A. Sharaf, Advances in Materials Science and Engineering (2016) http://dx.doi.org/10.1155/2016/3183909.

[9] W. G. C. Kumarage, L. B. D. R. P. Wijesundara, V. A. Seneviratne, C. P. Jayalath and B.

S. Dassanayake, Procedia Engineering, 139, 64 (2016).
[10] Z. S. Sopan and D. R. Narayan, International Journal of Science and Research, 4, 3, 1708 (2015)
[11] X. Shen, A. Yuan, F. Wang, J. Hong and Z. Xu, Solid State Communications, 133(1), 19 (2005).
[12] S. J. Ikhmayies, H. K. Juwhari and R. N. Ahmad-Bitar, Journal of Luminescence, 141, 27 (2013).
[13] N. R. Paudel, K. A. Wieland and A. D. Compaan, Sol. Energ. Materi. Sol. Cell, 105, 109 (2012).
[14] P. J. Sebastian and M. E. Calixto, Thin Solid Films, 360 (1-2), 128 (2000).
[15] A. A. Ziabari and F. E. Ghodsi, Sol. Energ. Materi. Sol. Cell, 105, 249 (2012).
[16] J. Schaffner, E. Feldmeier, A. Swirschuk, H. J. Schimper, A. Klein and W. Jaegermann, Thin Solid Films, 519, 7556 (2011).
[17] D. G. Diso, G. E. A. Muftah, V. Patel and I. M. Dharmadasa, J. Electrochem. Soc., 157 (6), H647 (2010).
[18] M. Fathy, A. E. B. Kashyout, S. Elyamny, G. D. Roston and A. A. Bishara, Int. J. Electrochem. Sc., 9, 6155 (2014).
[19] H. Y. R. Atapattu, D. S. M. De Silva, K. A. S. Pathiratne and I. M. Dharmadasa, J. Mater. Sc.: Mater. Electron, 27, (5), 5415 (2016).
[20] H. I. Salim, O. I. Olusola, A. A. Ojo, K. A. Urasov, M. B. Dergacheva and I. M. Dharmadasa, J. Mater. Sc.: Mater. Electron., (2016). DOI: 10.1007/s10854-016-4629-8.
[21] M. Rami, E. Benamar, M. Fahoume, F. Chraibi and A. Ennaoui, M. J. Condensed Matter, 3 (1), 66 (2000).
[22] A. N. Abdul-Manaf, A. R. Weerasinghe, O. K. Echendu and I. M. Dharmadasa, J. Mater. Sc: Mater. Electron. 26 (4), 2418 (2015).
[23] H. Jun-feng, F. Gan-hua, V. Krishnakumar, L. Cheng and W. Jaegermann, J. Mater. Sc.: Mater. Electron, 24, 2695 (2013).
[24] R. G. Dhere, M. Bonnet-Wymard, E. Charlet, E. Peter, J. N. Duenow, J. V. Li, D. Kuciauskas and T. A. Gessert, Thin Solid Films, 519, 7142 (2011).
[25] X. Wu, Solar Energy, 77, 803 (2004).
[26] O. K. Echendu, F. Fauzi, A. R. Weerasinghe and I. M. Dharmadasa, Thin Solid Films, 556, 529 (2014).
[27] B. M. Basol and B. McCandless, Journal of Photonics for Energy, 4, 040996-1 (2014).
[28] O. K. Echendu and I. M. Dharmadasa, J. Electron. Mater. , 43 (3), 791 (2014).
[29] N. B. Chaure, S. Bordas, A. P. Samantilleke, S. N. Chaure, J. Haigh and I. M. Dharmadasa, Thin Solid Films, 437, 10 (2003).
[30] W. J. Danaher, L. E. Lyons and G. C. Morris, Solar Energy Materials, 2, 137 (1985).

Figure Captions

Fig. 1 (a) Two-electrode cyclic voltammogram of CdS deposition electrolyte containing 0.3M $CdCl_2.H_2O$ + 0.03M $Na_2S_2O_3.5H_2O$ at a pH of 1.80±0.02 and temperature of (80±2)˚C. (b) Expansion of the area around the potential axis for clarity

Fig. 2 The graph of measured thickness vs. deposition time for the five electrodeposited CdS thin films. Straight line represents the expected theoretical trend from Faraday's law

Fig. 3 XRD patterns of (a) as-deposited and (b) annealed CdS thin films deposited at cathode voltage of 1450 mV and temperature of 80°C for different durations producing different thicknesses

Fig. 4 Absorbance spectra of (a) as-deposited and (b) annealed CdS films of different thicknesses grown for different durations

Fig. 5 (a) Transmittance vs. Wavelength for (a) as-deposited and (b) annealed CdS films of different thicknesses grown for different durations

Fig. 6 Reflectance spectra of the (a) as-deposited and (b) annealed CdS films of different thicknesses grown for different durations

Fig. 7 Absorption coefficient, α vs. Photon energy for (a) as-deposited and (b) annealed CdS thin films with different thicknesses deposited for different durations

Fig. 8 Graph of $(\alpha hv)^2$ vs. photon energy for (a) as-deposited and (b) annealed CdS thin films of different thicknesses deposited for different durations

Fig. 9 Extinction coefficient vs. Photon energy for (a) as-deposited and (b) annealed CdS thin films of different thicknesses deposited for different durations

Fig. 10 Dependence of refractive index, n with photon energy for (a) as-deposited and (b) annealed CdS thin films respectively

Fig. 11 (a) Real dielectric constant, ϵ_r vs. photon energy for (a) as-deposited and (b) annealed CdS films of different thicknesses deposited for different durations

Fig. 12 Imaginary dielectric constant, ϵ_i vs. photon energy for (a) as-deposited and (b) annealed CdS thin films of different thicknesses deposited for different durations

Fig. 13 SEM images of as-deposited (AD) and annealed (HT) CdS samples grown for different durations with different thicknesses. $CdCl_2$ treatment was done with saturated $CdCl_2$ in de-ionised water

Fig. 14 Percentage S and Cd atomic compositions of CdS films deposited for different durations

Effects of deposition time and post-deposition annealing on the physical and chemical properties of electrodeposited CdS thin films for solar cell application

O. K. Echendu[*1,2], U. S. Mbamara[2], K. B. Okeoma[2], C. Iroegbu[2], C. A. Madu[2], , I. C. Ndukwe[2] and I. M. Dharmadasa[1]

[1]Electronic Materials and Sensors Group, Materials and Engineering Research Institute,

Sheffield Hallam University, S1 1WB, Sheffield, UK.

[2]Thin Film Research Group, Department of Physics, Federal University of Technology,

P. M. B. 1526, Owerri, Nigeria.

*Corresponding author's email: oechendu@yahoo.com

Abstract

CdS thin films were cathodically electrodeposited by means of a two-electrode deposition system for different durations. The films were characterised for their structural, optical, morphological and compositional properties using x-ray diffraction (XRD), spectrophotometry, scanning electron microscopy (SEM) and energy dispersive x-ray (EDX) respectively. The results obtained show that the physical and chemical properties of these films are significantly influenced by the deposition time and post-deposition annealing. This influence manifests more in the as-deposited materials than in the annealed ones. XRD results show that the crystallite sizes of the different films are in the range (9.4 – 65.8) nm and (16.4 – 66.0) nm in the as-deposited and annealed forms respectively. Optical measurements show that the absorption coefficients are in the range $(2.7\times10^4 – 6.7\times10^4)$ cm^{-1} and $(4.3\times10^4 – 7.2\times10^4)$ cm^{-1} respectively for as-deposited and annealed films. The refractive index is in the range (2.40 – 2.60) for as-deposited films and come to the value of 2.37 after annealing. The extinction coefficient varies in the range (0.1 – 0.3) in as-deposited films and becomes 0.1 in annealed films. The estimated energy bandgap of the films is in the range (2.48 – 2.50) eV for as-deposited films and becomes 2.42 eV for all annealed films. EDX results show that all the films are S-rich in chemical composition with fairly uniform Cd/S ratio after annealing. The results show that annealing improves the qualities of the films and deposition time can be used to control the film thickness.

Keywords: Electrodeposition; two-electrode system; CdS; annealing; deposition time; thin-film.

Acknowledgement

The authors thank F. Fauzi, A. N. Abdul-Manaf, M. L. Madugu, I. O. Olusola and A. Ojo for valuable discussions. The principal author wishes to thank the Tertiary Education Trust Fund TETFUND), Nigeria and the Federal University of Technology, Owerri, Nigeria for financial support.

1.0 Introduction

CdS is a wide bandgap semiconductor with a direct bulk bandgap value of 2.42 eV [1]. It has desirable qualities that make it find use in applications such as solar cells (where it is used as a window or buffer material) [2, 3, 4], photoresistors, phosphors, electroluminescence [5], diodes [6], thin film transistors [7] and radiation detectors [8].

To produce CdS, different techniques have been used by different researchers. These include chemical bath deposition (CBD) [9], vacuum evaporation [10] chemical vapour deposition [11], spray pyrolysis [12], sputtering [13], screen printing [14], sol-gel [15], close space sublimation [16] and electrodeposition [17 - 20]. The electrodeposition of CdS has always been reported in the past based on the conventional three-electrode configuration [21] as is common in the electrodeposition of semiconductors. In recent times however, only a few reports on the use of two-electrode system for the electrodeposition of CdS can be found in the literature [17, 20, 22]. Two major reasons for the use of two-electrode system in the electrodeposition of semiconductors include: (i) to prevent any possible contamination of the deposition electrolyte by ions such as Ag^+ and K^+ which may eventually leak into the deposition electrolyte from the commonly used Ag/AgCl and Hg/HgCl (saturated calomel) reference electrodes during the electrodeposition process especially as the reference electrode ages; (ii) to simplify the electrodeposition process and therefore reduce cost.

For CdS/CdTe solar cell fabrication, for example, the CBD process has commonly been used to grow CdS thin films [23 - 25] while CdTe is deposited using CSS [23 - 25], sputtering [13] or electrodeposition [26, 27]. Due to the nature of CBD as a batch process, a lot of Cd-containing waste is generated in the large-scale deposition of CdS. This raises serious environmental concern as well as costs huge sums of money in order to manage and dispose of the waste. This situation poses a problem in a production line, coupled with the use of at least two different deposition techniques. This eventually results in the production of expensive solar panels. In such an industrial process, it is preferable to have only one production line by using only one technique to deposit both CdS and CdTe. A continuous process such as electrodeposition fits into this picture for the production of less expensive solar panels. Based on these reasons, the electrodeposition of CdS thin-films using two-electrode system has been undertaken and reported in this work for possible application in development of all-electrodeposited CdS/CdTe solar cells and other CdS-based devices.

The relevant equations used for deducing the optical parameters (from transmittance and absorbance measurements) of the CdS films are given in (1) – (8) as reported previously [28] below. It is well-known that when light is incident on a thin film material, it is either absorbed, transmitted or reflected, and the sum of the fractions of the absorbed, transmitted and reflected light equals unity, so that

$$A + T + R = 1 \quad (1)$$

where A is absorbance, T is transmittance and R is reflectance.

The overall response of the material to the incident light is connected to its refractive index according to equation (2).

$$N = n + iK \quad (2)$$

where N is the refractive index of the material, n is the real part of the refractive index and K is the imaginary part of the refractive index, also known as the extinction coefficient of the material in question.

The reflectance of the material and the real part of the refractive index are connected by equation (3).

$$R = \frac{(n-1)^2}{(n+1)^2} \quad (3)$$

The absorption coefficient α, of the material is also related to the extinction coefficient according to equation (4).

$$\alpha = \frac{4\pi K}{\lambda} \quad (4)$$

The complex dielectric constant ε, is related to n and K according to equation (5).

$$\varepsilon = (n + iK)^2 = \varepsilon_r + \varepsilon_i \quad (5)$$

where ε_r and ε_i are the real and imaginary parts of the dielectric constant of the material respectively.

The absorbance of the thin film is related to its transmittance according to equation (6).

$$A = \log_{10}\left(\frac{1}{T}\right) \quad (6)$$

The absorption coefficient is also related to the transmittance by

$$\alpha = -\ln\left(\frac{T}{d}\right) \quad (7)$$

where d is the thickness of the film.

Finally, for a direct bandgap semiconductor, such as CdS, the absorption coefficient is related to the energy hv, of the absorbed photons and the bandgap energy E_g, of the semiconductor by

$$\alpha = \frac{C\left(hv - E_g\right)^{1/2}}{hv} \qquad (8)$$

Where C is a constant, h is Planck's constant and v is the frequency of the incident photons.

2.0 Experimental procedure

2.1 Preparation of CdS deposition electrolyte

The CdS deposition electrolyte is made up of 0.3 M $CdCl_2.H_2O$ and 0.03 M $Na_2S_2O_3.5H_2O$ in 800 ml of de-ionised water. Both chemicals are laboratory reagent grade purchased from Fisher Scientific, United Kingdom. Before the addition of $Na_2S_2O_3.5H_2O$, the solution containing only $CdCl_2.H_2O$ was stirred for 24 hours to ensure proper dissolution of the $CdCl_2.H_2O$ crystals. The pH of the solution was then adjusted to 1.80±0.02 by adding some drops of dilute HCl. Afterwards, the $CdCl_2.H_2O$ solution was heated to a temperature of (80±2)ºC with stirring at 400 rotations per minute (r.p.m.). A cyclic voltammetry of the electrolyte was then taken using a computerised Gill AC potentiostat (ACM Instruments, Cumbria, UK) in two-electrode configuration, with a clean fluorine-doped tin oxide-coated glass (glass/FTO) as the working electrode and a high-purity carbon rod as the counter electrode. This was done in order to identify the deposition potential of Cd which has a standard reduction potential of -403 mV. From the result of the cyclic voltammetry, the $CdCl_2.H_2O$ electrolyte was electro-purified for 48 hours at a cathodic potential slightly lower than the deposition potential of Cd. This is usually done to get rid of possible ionic impurities present in the $CdCl_2.H_2O$ considering also the higher concentration of $CdCl_2.H_2O$ relative to $Na_2S_2O_3.5H_2O$.

After electro-purification, the 0.03 M $Na_2S_2O_3.5H_2O$ was added into the purified $CdCl_2.H_2O$ solution and stirred for about 6 hours. The pH of the resulting CdS deposition electrolyte was again adjusted to 1.80±0.02 using dilute HCl and NH_4OH. Another cyclic voltammetry was carried out, this time, to identify the range of possible deposition potentials for CdS. The voltammogram (which is the graph of current density vs. applied cathodic potential) for the CdS deposition electrolyte was then plotted as shown in figure 1 from which the possible cathodic deposition potential of CdS was identified to be in the range (1300 – 1500) mV.

2.2 Substrate preparation and electrodeposition of CdS thin films

The glass/FTO substrates used for both cyclic voltammetry and deposition of CdS thin films were cut from a large plate of dimension 30 cm×30 cm×3.0 mm into smaller sizes of dimension 3.0 cm×2.0 cm×3.0 mm. These were cleaned first with soap solution for 15 minutes in an ultrasonic bath. After rinsing with de-ionised water, they were again cleaned with acetone and methanol in turn while rinsing with de-ionised water in-between. Finally, they were dried in a stream of N_2.

To carry out the electrodeposition of CdS, each small glass/FTO substrate was attached to a carbon plate using insulating PTFE tape, and this served as the working electrode or cathode. The same potentiostat used for cyclic voltammetry in two-electrode configuration was used in depositing CdS onto the substrates. In order to determine the best deposition potential for CdS, some preliminary samples were deposited on glass/FTO at different potentials across the initially identified deposition potential range of 1300 mV – 1500 mV, and characterised using x-ray diffraction (XRD) and spectrophotometry. From this, the best cathodic electrodeposition potential for CdS under the conditions described was identified as 1450 mV.

Five CdS thin films were then carefully deposited on glass/FTO at this potential for different durations of 5 minute, 10 minutes, 15 minutes, 20 minutes and 25 minutes, in order to study the effect of deposition time on the properties of the films. After deposition, each sample was rinsed with de-ionised water, dried in a flow of nitrogen and then cut into two equal parts. One set of these parts was designated 'as-deposited' samples while the other set was treated with $CdCl_2$ by dipping them in a saturated solution of $CdCl_2$ in de-ionised water and drying them in air. Afterwards, they were heat-treated at 400 ºC for 20 minutes in a furnace and allowed to cool in air atmosphere. These were designated 'annealed' samples.

2.3 Characterisation of the deposited CdS thin films

The characterisation of the as-deposited and annealed CdS thin films was done using Philips X'Pert Pro x-ray diffraction system (Philips Analytical, Almelo, Australia) for structural properties, Cary 50 UV-VIS spectrophotometer (Varian, Australia Pty Ltd) for optical properties, FEG NOVA NANO scanning electron microscope (FEI Company, The Netherlands) for morphological properties and energy dispersive x-ray (EDX) using EDX detector (Oxford Instruments, UK) attached to the SEM equipment. Thicknesses of the films were measured using UBM Microfocus optical measuring system (UBM, Messetechnik GmbH, Ettlingen, Germany). The results of the characterisation of these films are presented in the following section.

3.0 Results and discussion

3.1 Effect of deposition time on thickness of electrodeposited CdS thin films

Figure 2 shows the effect of deposition time on the thickness of the five electrodeposited CdS thin film samples. The figure shows that the thickness of deposited CdS layers increases as deposition time increases. This relationship is however not linear. The reason for this nonlinearity is not far-fetched. The condition of the deposition bath at the time of growth of each sample plays a significant role. Experience shows that because of the problem of sulphur precipitation, especially at elevated temperatures like the ones used in this experiment the concentration of sulphur in the deposition electrolyte runs low very easily. This usually manifests in drop in the deposition current density and therefore the deposition rate. To try to restore the concentration of sulphur in the electrolyte, a calculated amount of the sulphur source ($Na_2S_2O_3$)

is usually added to the bath from time to time and the deposition current density is controlled by adjusting the stirring rate. This could explain the fluctuation observed in the thickness of the samples under constant temperature and deposition potential since the manual addition of the S^{2-} source may not be very precise.
The same thing could happen with Cd^{2+} but to bring this situation under control, and as a trick in electrodeposition, the initial concentration of Cd^{2+} is made higher (10 times higher in this case) than that of S^{2-} in the electrolyte. This is one of the reasons why the ratio of the concentration of these two ions in the bath is $[Cd^{2+}] / [S^{2-}] = 10 / 1$.

3.2 Effect of deposition time and annealing on the structural properties of the CdS thin films - X-ray diffraction study

Figures 3 (a) and (b) show the XRD patterns of the five electrodeposited CdS thin films, before and after annealing respectively. Looking at the figures, up to a deposition time of 10 minutes, the XRD features did not show up clearly, suggesting that the material at this early formation stage is either weakly crystalline and/or very thin. From 15 minutes of growth and above, the material begins to crystallise and become thicker, and the XRD peaks begin to show up more clearly. A possible reason for this observed poor crystalline (or rather amorphous) nature of CdS at the initial nucleation and formation stage is the fact that the formation of sulphur atoms starts first at the cathode before the formation of Cd atoms begins. This prior formation of sulphur then helps to drive the deposition of Cd. At the initial stage therefore more sulphur gets deposited on the cathode with only very little amount of Cd. As the deposition progresses in time, more and more Cd is attracted to and deposited on the cathode leading to the formation of CdS with increased Cd-content as the two species react together at the cathode. As a result, CdS peaks begin to show up in the XRD at these elevated growth times.

Table 1 shows the structural parameters of the deposited CdS films extracted from the XRD data. The fact that the deposition of CdS on the substrate is still at the nucleation/formation stage is evident in lack of some structural parameters as shown in Table 1 for the films grown for 5 – 10 minutes. As the deposition time increases, all the structural parameters corresponding to the respective XRD peaks begin to show up clearly. The XRD results shown in figure 3 and Table 1 closely match the standard reference Joint Committee on Powder Diffraction and Standards (JCPDF) file no. 01-075-1545. This file has the 2θ and d-spacing values for the three main XRD peaks of hexagonal CdS as follows: [$2\theta = 24.80^{o}$; d-spacing = 3.587 Å]; [$2\theta = 26.49^{o}$; d-spacing = 3.362 Å]; [$2\theta = 28.17^{o}$; d-spacing = 3.165 Å].

A close look at the data in Table 1 shows that with the exception of the sample grown for 10 minutes, for the same reasons stated above, all samples exhibit an increase in the d-spacing values and a decrease in the 2θ values. This is an indication of the presence of tensile stress on the crystal planes and the crystallites. Based on the three main XRD peaks of the hexagonal CdS, only the samples grown for 15 minutes and 20 minutes show constant crystallite sizes before and

after annealing for two out of the three 2θ angles simultaneously. The optimum deposition time for CdS under the conditions used in the present work could therefore be in the range of 15 – 20 minutes.

Table 1: Structural parameters of the CdS thin films extracted from XRD measurements.

	As-deposited				Annealed			
Growth Time (min)	2θ (°)	d-spacing (Å)	β (°)	D (nm)	2θ (°)	d-spacing (Å)	β (°)	D (nm)
5	- - - 26.24 - - -	- - - 3.397 - - -	- - - 0.1624 - - -	- - - 50.5 - - -	25.14 26.20 - - -	3.543 3.401 - - -	0.5196 0.1624 - - -	16.4 52.6 - - -
10	25.17 26.23 28.07	3.539 3.398 3.179	0.9092 0.1624 0.3247	9.4 52.6 26.4	- - - 26.21 28.00	- - - 3.400 3.287	- - - 0.1624 0.1299	- - - 52.6 66.0
15	24.64 26.24 28.09	3.613 3.397 3,177	0.1948 0.1948 0.1948	43.7 43.9 44.0	24.64 26.23 27.98	3.613 3.398 3.189	0.1948 0.1624 0.1948	43.7 52.6 44.0
20	24.67 26.23 28.08	3.609 3.397 3.178	0.1624 0.1624 0.2598	52.5 52.6 33.0	24.65 26.25 28.03	3.611 3.395 3.183	0.1948 0.1624 0.2598	43.7 52.6 33.0
25	24.62 26.19 28.05	3.616 3.403 3.181	0.1948 0.1299 0.2598	43.7 65.8 33.0	24.55 26.18 27.95	3.626 3.404 3.193	0.1948 0.2273 0.1948	43.7 37.6 44.0

3.3 Effect of deposition time and annealing on the optical properties of CdS thin films – Spectrophotometry study

In this section the results of the effect of growth time and annealing on optical properties of the five electrodeposited CdS thin films under study are presented. Figures 4 (a) and (b) show the absorbance spectra of these samples before and after post-deposition annealing respectively.

Figure 4 (a) shows large scatter in the absorbance of the as-deposited films. The films also show significant absorbance in the long wavelength region with weak absorbance edges. In the annealed samples (fig 4 (b)), the absorbance curves show more defined absorbance edges with reduced spread in absorbance. There is also considerable reduction in the absorption of photons (over 50%) in the long wavelength region of the spectrum especially for the thicker samples. The raised absorption tail in the (for the thicker) as-deposited samples indicates the presence of significant amount of photon scattering in these materials. This may be due to the presence of mixed phases, poor stoichiometry and strain/stress in the samples as was pointed out earlier in the XRD study. After annealing, CdS materials with improved qualities are obtained with

significantly reduced scattering, hence the results in figure 4 (b).

Figures 5 (a) and (b) show the transmittance spectra of the as-deposited and annealed CdS films of different deposition times/thicknesses respectively. In both figures, one observes that transmittance decreases as film thickness increases. Also transmittance increases as incident photon wavelength increases. For films with thicknesses ≥201 nm, there is little or no significant transmission of light in the lower wavelengths up to 480 nm. However, for the thinnest sample with thickness of 127 nm, there is relatively significant transmission of photons in this wavelength range with up to 50% transmittance. This, in addition to the high absorption coefficient of CdS, explains the reason why it has been said by some researchers that for application in solar cells as window material, CdS needs to have very small thickness, even as small as (10 - 50) nm [1]. The problem in this situation however, is the issue of good coverage of the underlying TCO substrate. If the thickness of CdS is too low, it may not properly cover the TCO surface and this leads to short-circuiting when an absorber material such as CdTe is deposited on CdS for solar cell fabrication, for example. However, if the particular CdS used is highly photoactive, then very thin layer is not necessary as absorption of photons by the CdS layer helps to create more photo-generated charge carriers.

A close observation of figures 5 (a) and (b) shows that the transmittance spectra in the as-deposited CdS films show wider spread in the entire wavelength range under consideration compared to those of the annealed films. This also points to the fact that the optical quality of these films is improved by post-deposition annealing, since electrodeposition is a low-temperature deposition technique (usually done at temperatures lower than 100 ºC in aqueous solution) compared to other advanced semiconductor growth techniques.

Figures 6 (a) and (b) show the variation of reflectance with photon wavelength for the as-deposited and annealed CdS thin films respectively. Both figures show that the reflectance, of all the films has a maximum value of 20%. However, the photon wavelength at which this maximum occurs is strongly thickness (and therefore growth time)-dependent, and this dependence is more profound in the as-deposited films. The annealed films have less spread in the wavelength at which reflectance sets in compared to as-deposited films. As the thickness of the layer increases, this reflectance maximum, as well as the onset of reflectance, shifts towards longer wavelengths.

Towards the longer wavelengths from the point of maximum reflectance, the reflectance falls rapidly. This result shows that if a very thin CdS film (thickness in the range ≤ 127 nm) is used as a window layer for example in CdS/CdTe solar cell, there will be significant reflection of the incident photons in the short wavelength regions back into the atmosphere by the thin CdS layer. It is known that photons in this wavelength range cause thermalisation in solar cells as a result of their high energy content. Using very thick CdS layer (thickness in the range > 127 nm) again will result in the reflection of significant amount of photons in the visible region. There should

therefore be a balance somewhere in-between, requiring an optimum thickness of CdS for this kind of application.

Figures 7 (a) and (b) show the graphs of absorption coefficient, α vs. photon energy ($h\nu$) for the as-deposited and annealed CdS thin films respectively. Both figures show similar trend in the dependence of absorption coefficient on incident photon energy. Like in figure 5, the absorption edges are very weak in the as-deposited films (figure 7 (a)), but become sharper after annealing (figure 7 (b)). The spread in the absorption coefficient values is also wider in the as-deposited films compared to the annealed films. Careful observation shows that there is a gradual shift in the absorption coefficient edge of the as-deposited films towards shorter wavelength as film thickness increases, and the absorption coefficient tends to increase with film thickness.
These trends are however not clear in the annealed films as the absorption coefficients of the films tend to close up together, up to the photon energy values where the absorption curve has the highest gradient. From figures 7 (a) and (b), the absorption coefficients of these films in the vicinity of the bandgap energy of CdS (2.42 eV - 2.50 eV) lie in the range (2.7×10^4 – 6.7×10^4) cm^{-1} for as-deposited films and (4.3×10^4 - 7.2×10^4) cm^{-1} for annealed samples. These values are in agreement with literature values for CdS grown by CBD [29, 30].

Figures 8 (a) and (b) show the graphs of $(\alpha h\nu)^2$ vs. photon energy for the as-deposited and annealed CdS films respectively, for the purpose of estimating the energy bandgaps of the films. From figure 8, one observes that the as-deposited CdS films show higher values of $(\alpha h\nu)^2$ than the annealed films. The energy bandgap values estimated from figure 8 (a) for the as-deposited films are in the range (2.48 – 2.50) eV while the bandgaps of the annealed films all come to the same value of ~2.42 eV as seen in figure 8 (b). Around the energy bandgaps, the values of $(\alpha h\nu)^2$ for the as-deposited films roughly increase as film thickness increases, while the trend is not clear for the annealed films.

Figures 9 (a) and (b) show the dependence of extinction coefficient, K on photon energy for the as-deposited and annealed CdS thin films respectively. Figures 9 (a) and (b) follow the trend in absorption coefficient (figure 7), with the as-deposited films displaying higher K-values in the vicinity of the bandgap in the range (0.1 – 0.3) than annealed films whose corresponding K-values come to the value of ~0.1. The extinction coefficient generally increases as photon energy increases for both groups of samples. This shows that incident light will travel farther in the annealed films before getting completely absorbed than in the as-deposited films. Figure 9 (a) shows that K-values roughly increase with film thickness which suggests that incident photons will travel farther in thinner samples before getting completely absorbed.

Figures 10 (a) and (b) show the dependence of refractive index, n with photon energy for the as-deposited and annealed CdS thin films respectively. The refractive index shows maximum values of 2.40 - 2.60 for the as-deposited films and a maximum value of ~2.37 for annealed samples in

the vicinity of the bandgap energy of CdS for all the layers. This shows the improvement and uniformity in the quality of all the films after annealing. In general, as one goes towards higher photon energies, the cut-off value of the refractive index increases as film thickness decreases. The refractive index generally follows a sort of parabolic trend with a maximum. Looking at the annealed films in figure 10 (b), it is seen that below the bandgap energy of the films, the refractive index decreases. Above the bandgap energy, n falls more rapidly. The only exception to this particular trend is the thinnest layer with thickness of 127 nm in which n rather falls very slowly beyond the bandgap energy of CdS. This suggests that there is significant scattering of light of shorter wavelengths in this particular material in line with the observation in the reflectance.

Figures 11 (a) and (b) show the real dielectric constants of the as-deposited and annealed CdS thin films of different thicknesses respectively. The real dielectric constant, ϵ_r has the same feature as the refractive index showing a maximum value of 1.5 – 6.9 for as-deposited films and a value of 6.9 for all the annealed films. The photon energy corresponding to maximum ϵ_r values in each set of films varies slightly according to the thickness of the films; the thicker the film, the lower this energy value. Again, towards lower energy values, from the bandgap energy, the ϵ_r values fall gradually while towards higher energy values, they fall more rapidly. The implication of this behaviour is that these films will exhibit higher capacitive properties in the lower photon energy region than in the higher energy region.

Figures 12 (a) and (b) show the graphs of imaginary dielectric constant, ϵ_i vs. photon energy for as-deposited and annealed CdS thin films respectively. There is no specific trend in the variation of the imaginary dielectric constant with film thickness across the photon energy range under consideration, especially for the as-deposited films. However, the imaginary dielectric constant, ϵ_i in figure 12 (b) decreases as the film thickness increases in the energy region below the bandgap value of the layers. For each layer however, ϵ_i increases with increasing photon energy reaching a maximum value at a certain photon energy beyond which it falls rapidly. This maximum point varies with film thickness slightly towards higher energy as the film thickness decreases. The sample with thickness of 127 nm again displays a different behaviour beyond this maximum energy point. The value of ϵ_i for this layer tends to increase beyond this energy reaching another higher maximum value around photon energy of 3.2 eV.

3.4 Effect of deposition time and annealing on the surface morphology of the CdS thin films - Scanning electron microscopy (SEM) study

Figure 13 shows the SEM images of the five CdS thin films of different thicknesses deposited for different durations. It can be seen that as the thicknesses of the films increase, the grains become clearer and more closely packed. At thicknesses of 127 nm and 201 nm however, the amount of deposited CdS material could not completely cover the FTO substrates. These two samples therefore show significant amount of gaps in-between CdS grains with some FTO grains clearly

exposed as shown. The application of CdS films of these thicknesses, for example, in the fabrication of glass/FTO/CdS/CdTe/metal solar cell or in other electronic devices, using the particular glass/FTO substrates in this work will definitely be a failure as a result of shunting of both CdTe and the metal contact with the FTO which will result in loss of fill factor and open-circuit voltage in solar cells and general poor performance of any other electronic device made with them.

Apart from the 377-nm film (corresponding to a growth time of 20 minutes), the other samples did not show any significant increase in grain size after post-deposition annealing. This suggests that this thickness may be the approximate optimum thickness for CdS based on grain size improvement after annealing for the particular glass/FTO substrates used.

3.5 Effect of deposition time and annealing on the atomic composition of the CdS thin films – EDX study

Table 2 and figure 14 show the percentage S and Cd compositions of the CdS thin films of different thicknesses deposited for different durations in both as-deposited and annealed forms.

Table 2: Percentage S and Cd atomic compositions of CdS films deposited for different durations in both as-deposited and annealed forms.

Vg (mV)	Sample ID	Deposition time (min)	Thickness (nm)	Atomic composition (%)				As-deposited Cd/S	Annealed Cd/S
				As-deposited		Annealed			
				Cd	S	Cd	S		
1450	CS148	5	127	42.2	57.8	39.9	60.1	0.73	0.51
1450	CS147	10	201	44.7	55.3	47.9	52.1	0.81	0.92
1450	CS146	15	295	48.1	51.9	48.8	51.2	0.93	0.95
1450	CS145	20	377	48.6	51.4	48.7	51.3	0.94	0.95
1450	CS144	25	557	48.5	51.5	48.6	51.4	0.94	0.95

The results show generally that as-deposited films are S-rich. As the deposition time (thickness) increases the S content decreases up to the thickness of about 377 nm (20 minutes growth time) and then begins to increase slightly as thickness increases beyond this point. After annealing, all the samples also emerged S-rich. Cd content is observed to decrease for the films grown for 5 minutes relative to its as-deposited form. Nevertheless, for the annealed samples, the Cd content gradually increases with growth time up to 15 minutes before gradually decreasing. The best stoichiometry after annealing comes for growth time in the range (15 - 25) minutes corresponding to thickness in the range (295 - 557) nm according to Table 2 and figure 14 (b). However, the 20 minutes sample (377 nm) and the 25 minutes sample appear to have the best

stoichiometry (Cd/S closest to unity) in both as-deposited and annealed forms.

4 Conclusion

The effects of deposition time and post-deposition annealing on the physical and chemical properties of electrodeposited CdS thin films have been presented. The electrodeposition of these films was carried out using two-electrode system for process simplification and cost reduction. Deposition time was seen to have significant influence on the structural, optical, morphological and chemical composition properties of the deposited CdS films under the conditions described. As the deposition time increased, thickness of the films increased. Increase in deposition time resulted in appearance of more and intense CdS XRD peaks. This also resulted in increased absorbance and reduced transmittance. The optical constants also varied significantly with deposition time/film thickness especially for the as-deposited films, while annealing tends to narrow the spread in these parameters. The morphology of the films showed that there is better coverage of the glass/FTO substrates as deposition time increased and the CdS grains became more compacted. Also, the Cd/S ratio in the as-deposited films gradually increased as deposition time increased while it remained fairly constant after annealing. Post-deposition annealing is generally observed to result in improvement of the physical and chemical properties of the films for all the deposition times/thicknesses considered.

Conflict of interest

The authors declare that they have no conflict of interest.

References

[1] T. M. Razykov, C. S. Ferekides, D. Morel, E. Stefanakos, H. S. Ullal and H. M. Upadhyaya, Solar Energy, 85, 1580 (2011).

[2] A. Bosio, N. Romeo, S. Mazzamuto and V. Canevari, Prog. Cryst. Growth & Charact. Mater., 52, 247 (2006).

[3] O. K. Echendu and I. M. Dharmadasa, Energies, 8, 4416 (2015).

[4] N. Naghavi, G. Renou, V. Bockelee, F. Donsanti, P. Genevee, M. Jubault, J. F. Guillemoles and D. Lincot, Thin Solid Films, 519 (21), 7600 (2011).

[5] Y. Kraftmankher, European Journal of Physics 33, 503 (2012).

[6] S. Guduru, V. P. Singh, S. Rajaputra, S. Mishra, R. Mangu and I. S. Omer, Thin Solid Films, 518, 7, 1809 (2010).

[7] W. Wondmagegn, I. Meiia, A. Salas-Villasenor, H. J. Stiegler, M. A. Quevedo-Lopez, R. J. Pieper and B. E. Gnade, Microelectronic Engineering, 157, 64 (2016).

[8] M. R. Balboul, A. Abdel-Galil, I. S. Yahia and A. Sharaf, Advances in Materials Science and Engineering (2016) http://dx.doi.org/10.1155/2016/3183909.

[9] W. G. C. Kumarage, L. B. D. R. P. Wijesundara, V. A. Seneviratne, C. P. Jayalath and B.

S. Dassanayake, Procedia Engineering, 139, 64 (2016).
[10] Z. S. Sopan and D. R. Narayan, International Journal of Science and Research, 4, 3, 1708 (2015)
[11] X. Shen, A. Yuan, F. Wang, J. Hong and Z. Xu, Solid State Communications, 133(1), 19 (2005).
[12] S. J. Ikhmayies, H. K. Juwhari and R. N. Ahmad-Bitar, Journal of Luminescence, 141, 27 (2013).
[13] N. R. Paudel, K. A. Wieland and A. D. Compaan, Sol. Energ. Materi. Sol. Cell, 105, 109 (2012).
[14] P. J. Sebastian and M. E. Calixto, Thin Solid Films, 360 (1-2), 128 (2000).
[15] A. A. Ziabari and F. E. Ghodsi, Sol. Energ. Materi. Sol. Cell, 105, 249 (2012).
[16] J. Schaffner, E. Feldmeier, A. Swirschuk, H. J. Schimper, A. Klein and W. Jaegermann, Thin Solid Films, 519, 7556 (2011).
[17] D. G. Diso, G. E. A. Muftah, V. Patel and I. M. Dharmadasa, J. Electrochem. Soc., 157 (6), H647 (2010).
[18] M. Fathy, A. E. B. Kashyout, S. Elyamny, G. D. Roston and A. A. Bishara, Int. J. Electrochem. Sc., 9, 6155 (2014).
[19] H. Y. R. Atapattu, D. S. M. De Silva, K. A. S. Pathiratne and I. M. Dharmadasa, J. Mater. Sc.: Mater. Electron, 27, (5), 5415 (2016).
[20] H. I. Salim, O. I. Olusola, A. A. Ojo, K. A. Urasov, M. B. Dergacheva and I. M. Dharmadasa, J. Mater. Sc.: Mater. Electron., (2016). DOI: 10.1007/s10854-016-4629-8.
[21] M. Rami, E. Benamar, M. Fahoume, F. Chraibi and A. Ennaoui, M. J. Condensed Matter, 3 (1), 66 (2000).
[22] A. N. Abdul-Manaf, A. R. Weerasinghe, O. K. Echendu and I. M. Dharmadasa, J. Mater. Sc: Mater. Electron. 26 (4), 2418 (2015).
[23] H. Jun-feng, F. Gan-hua, V. Krishnakumar, L. Cheng and W. Jaegermann, J. Mater. Sc.: Mater. Electron, 24, 2695 (2013).
[24] R. G. Dhere, M. Bonnet-Wymard, E. Charlet, E. Peter, J. N. Duenow, J. V. Li, D. Kuciauskas and T. A. Gessert, Thin Solid Films, 519, 7142 (2011).
[25] X. Wu, Solar Energy, 77, 803 (2004).
[26] O. K. Echendu, F. Fauzi, A. R. Weerasinghe and I. M. Dharmadasa, Thin Solid Films, 556, 529 (2014).
[27] B. M. Basol and B. McCandless, Journal of Photonics for Energy, 4, 040996-1 (2014).
[28] O. K. Echendu and I. M. Dharmadasa, J. Electron. Mater. , 43 (3), 791 (2014).
[29] N. B. Chaure, S. Bordas, A. P. Samantilleke, S. N. Chaure, J. Haigh and I. M. Dharmadasa, Thin Solid Films, 437, 10 (2003).
[30] W. J. Danaher, L. E. Lyons and G. C. Morris, Solar Energy Materials, 2, 137 (1985).

Figure Captions

Fig. 1 (a) Two-electrode cyclic voltammogram of CdS deposition electrolyte containing 0.3M $CdCl_2.H_2O$ + 0.03M $Na_2S_2O_3.5H_2O$ at a pH of 1.80±0.02 and temperature of (80±2)˚C. (b) Expansion of the area around the potential axis for clarity

Fig. 2 The graph of measured thickness vs. deposition time for the five electrodeposited CdS thin films. Straight line represents the expected theoretical trend from Faraday's law

Fig. 3 XRD patterns of (a) as-deposited and (b) annealed CdS thin films deposited at cathode voltage of 1450 mV and temperature of 80°C for different durations producing different thicknesses

Fig. 4 Absorbance spectra of (a) as-deposited and (b) annealed CdS films of different thicknesses grown for different durations

Fig. 5 (a) Transmittance vs. Wavelength for (a) as-deposited and (b) annealed CdS films of different thicknesses grown for different durations

Fig. 6 Reflectance spectra of the (a) as-deposited and (b) annealed CdS films of different thicknesses grown for different durations

Fig. 7 Absorption coefficient, α vs. Photon energy for (a) as-deposited and (b) annealed CdS thin films with different thicknesses deposited for different durations

Fig. 8 Graph of $(\alpha hv)^2$ vs. photon energy for (a) as-deposited and (b) annealed CdS thin films of different thicknesses deposited for different durations

Fig. 9 Extinction coefficient vs. Photon energy for (a) as-deposited and (b) annealed CdS thin films of different thicknesses deposited for different durations

Fig. 10 Dependence of refractive index, n with photon energy for (a) as-deposited and (b) annealed CdS thin films respectively

Fig. 11 (a) Real dielectric constant, ϵ_r vs. photon energy for (a) as-deposited and (b) annealed CdS films of different thicknesses deposited for different durations

Fig. 12 Imaginary dielectric constant, ϵ_i vs. photon energy for (a) as-deposited and (b) annealed CdS thin films of different thicknesses deposited for different durations

Fig. 13 SEM images of as-deposited (AD) and annealed (HT) CdS samples grown for different durations with different thicknesses. $CdCl_2$ treatment was done with saturated $CdCl_2$ in de-ionised water

Fig. 14 Percentage S and Cd atomic compositions of CdS films deposited for different durations

Fig.1

Click here to download Figure Fig1.doc

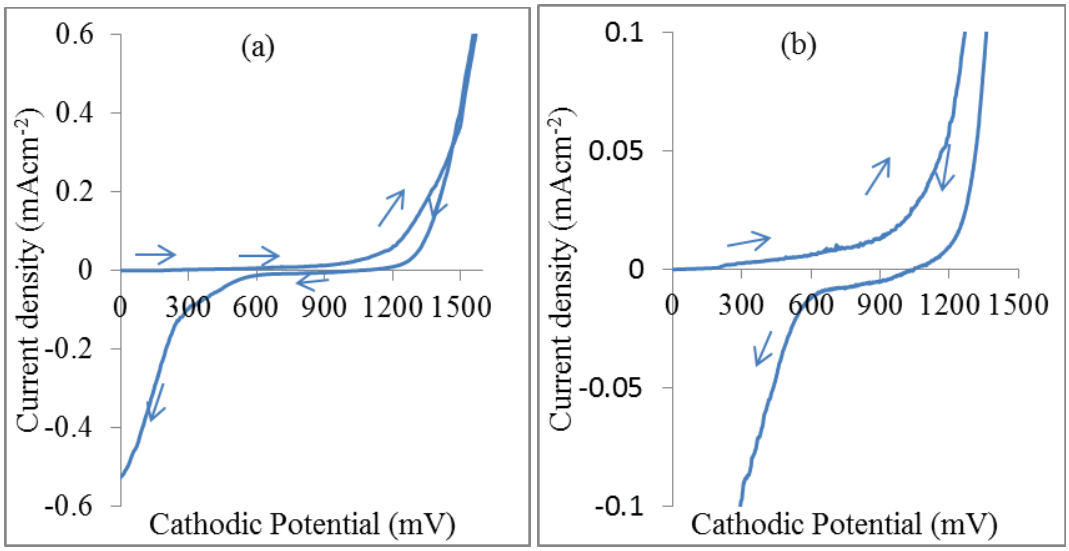

Fig. 1.xlxs

Fig.2

Click here to download Figure Fig2.doc

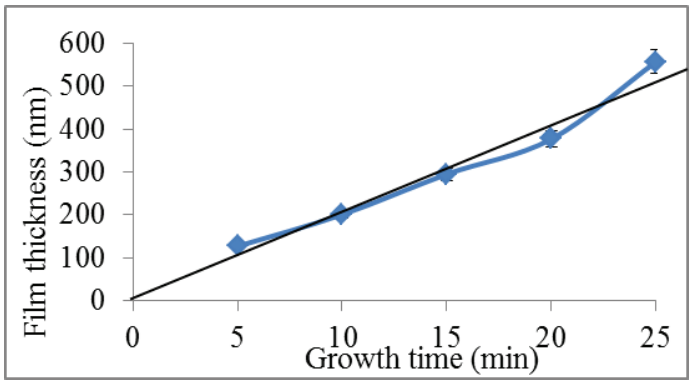

Fig.2.xlxs

Fig.3

Click here to download Figure Fig3.doc

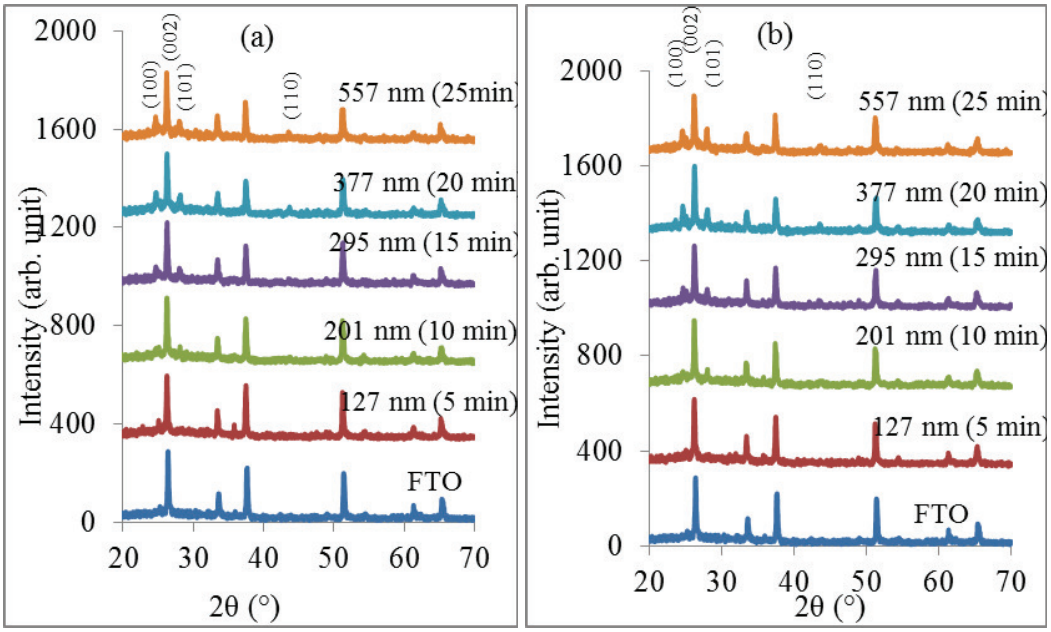

Fig3.xlxs

Fig.4

Click here to download Figure Fig4.doc

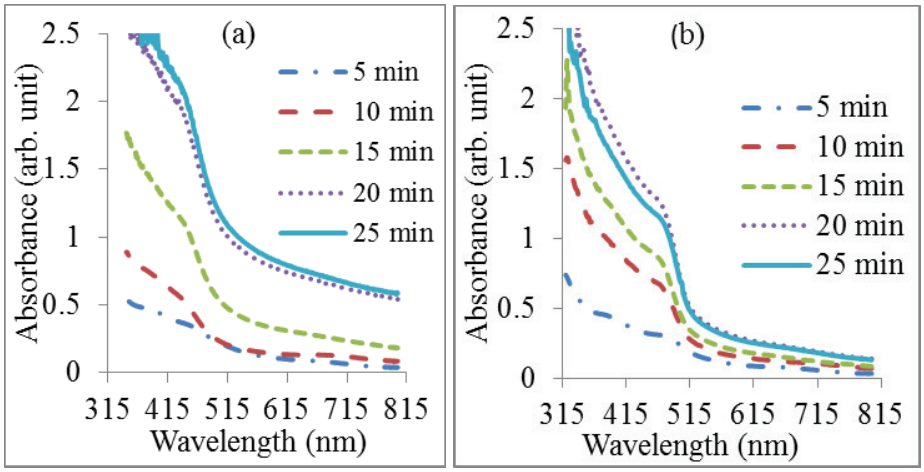

Fig4.xlx

Fig.5

Click here to download Figure Fig5.doc

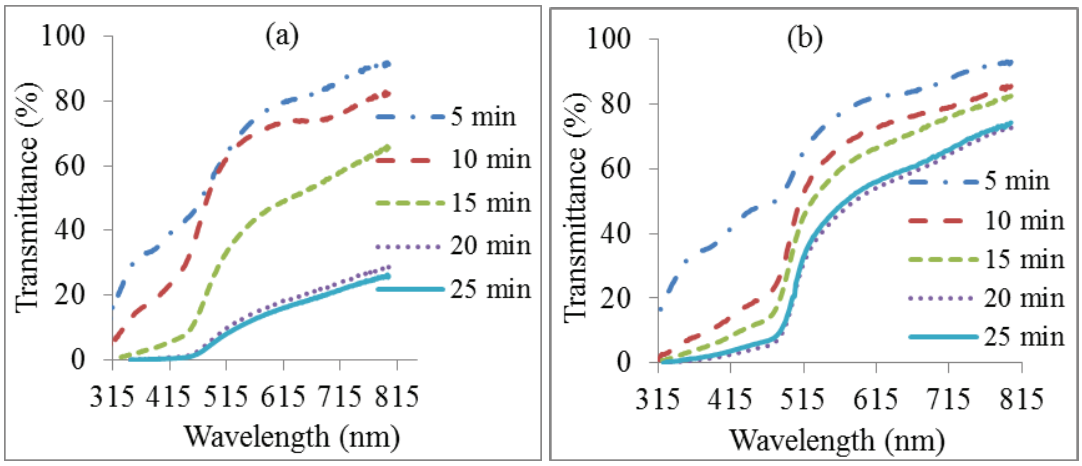

Fig5.xlxs

Fig.6

Click here to download Figure Fig6.doc

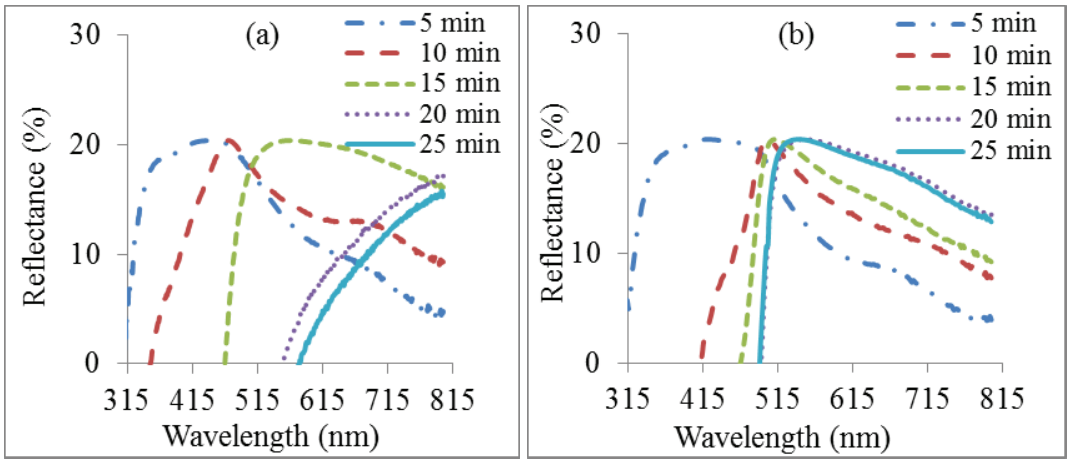

Fig6.xlxs

Fig.7

Click here to download Figure Fig7.doc

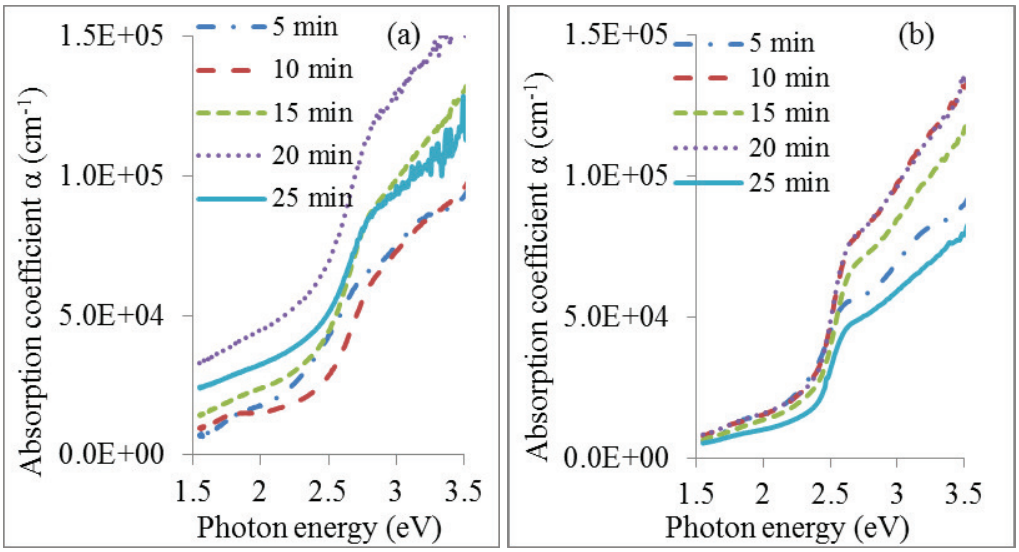

Fig7.xlxs

Fig.8

Click here to download Figure Fig8.doc

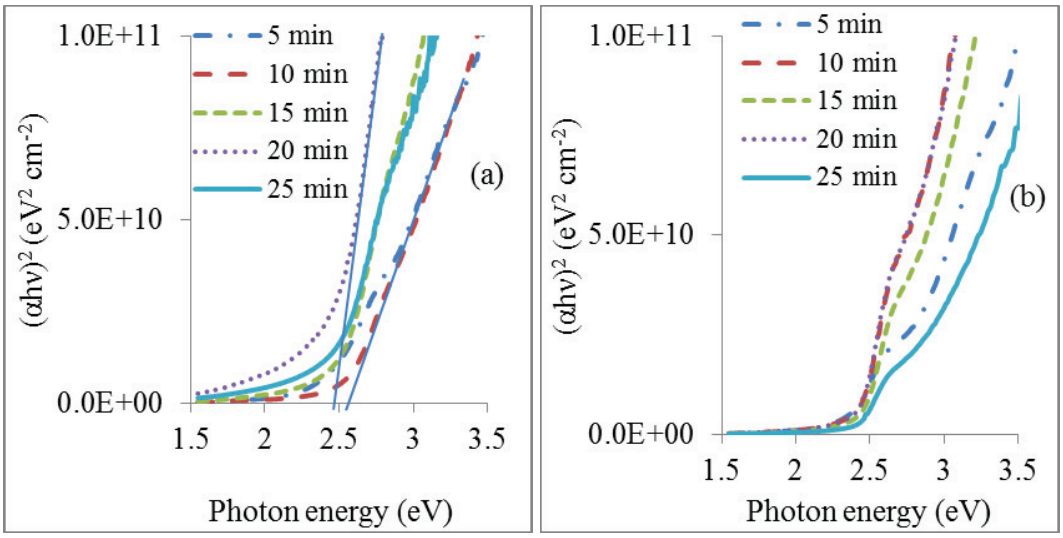

Fig8.xlxs

Fig.9

Click here to download Figure Fig9.doc

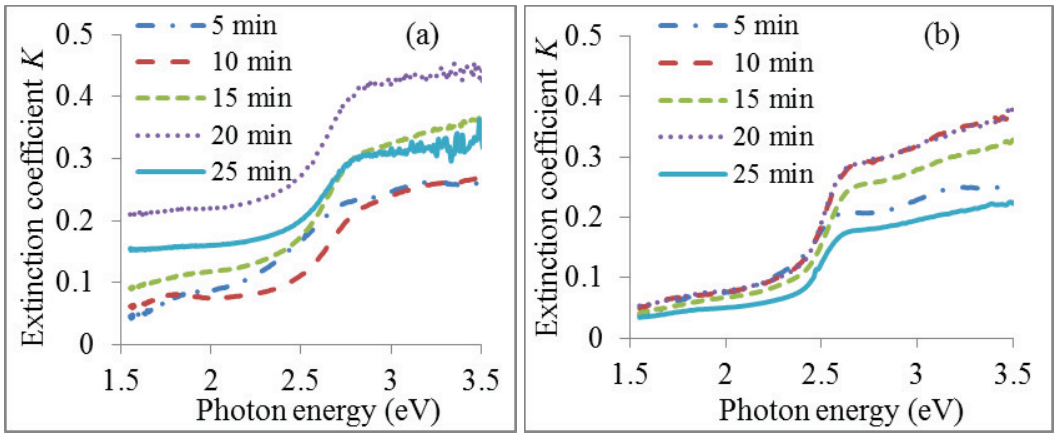

Fig9.xlxs

Fig.10

Click here to download Figure Fig10.doc

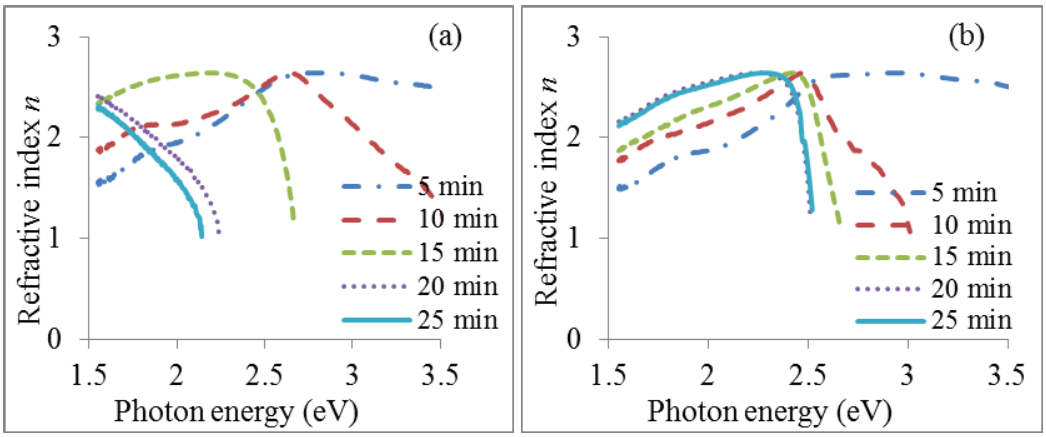

Fig10.xlxs

Fig.11

Click here to download Figure Fig11.doc

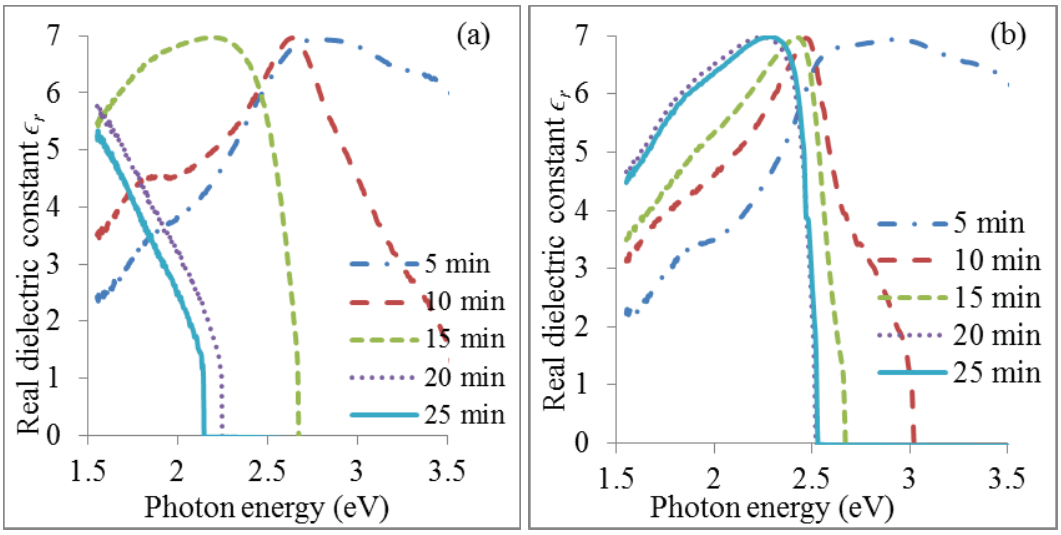

Fig11.xlxs

Fig.12

Click here to download Figure Fig12.doc

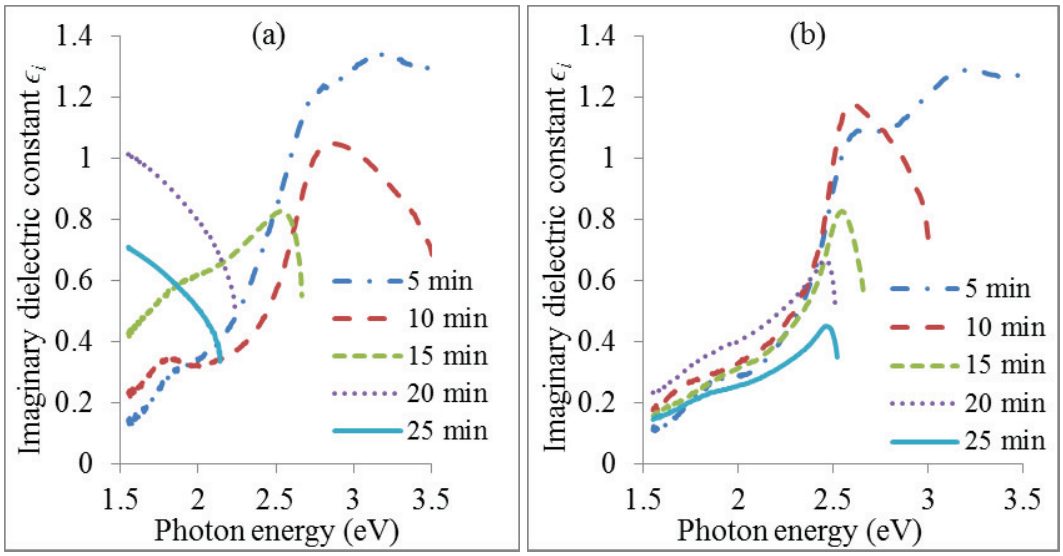

Fig12.xlxs

Fig.13

Click here to download Figure Fig13.doc

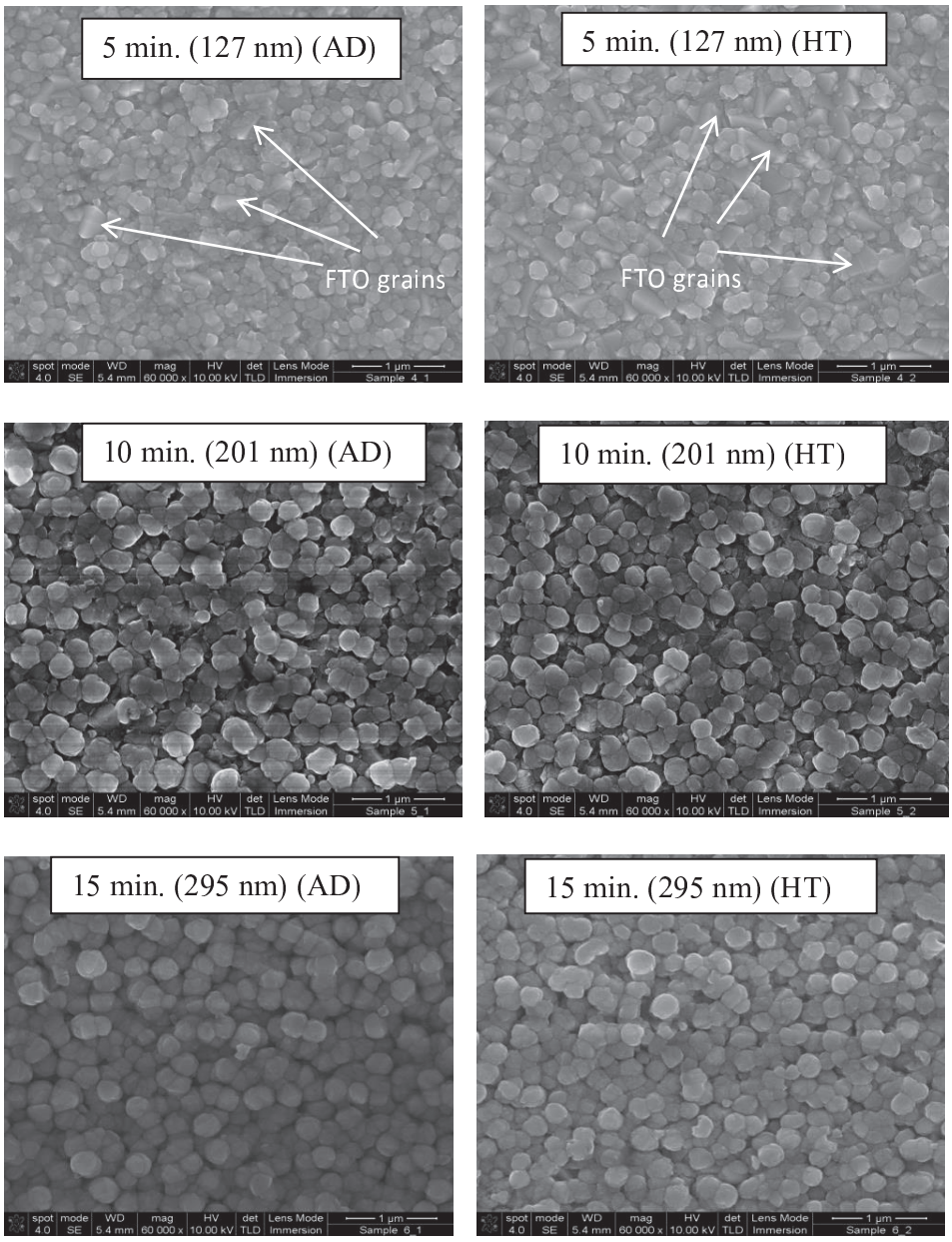

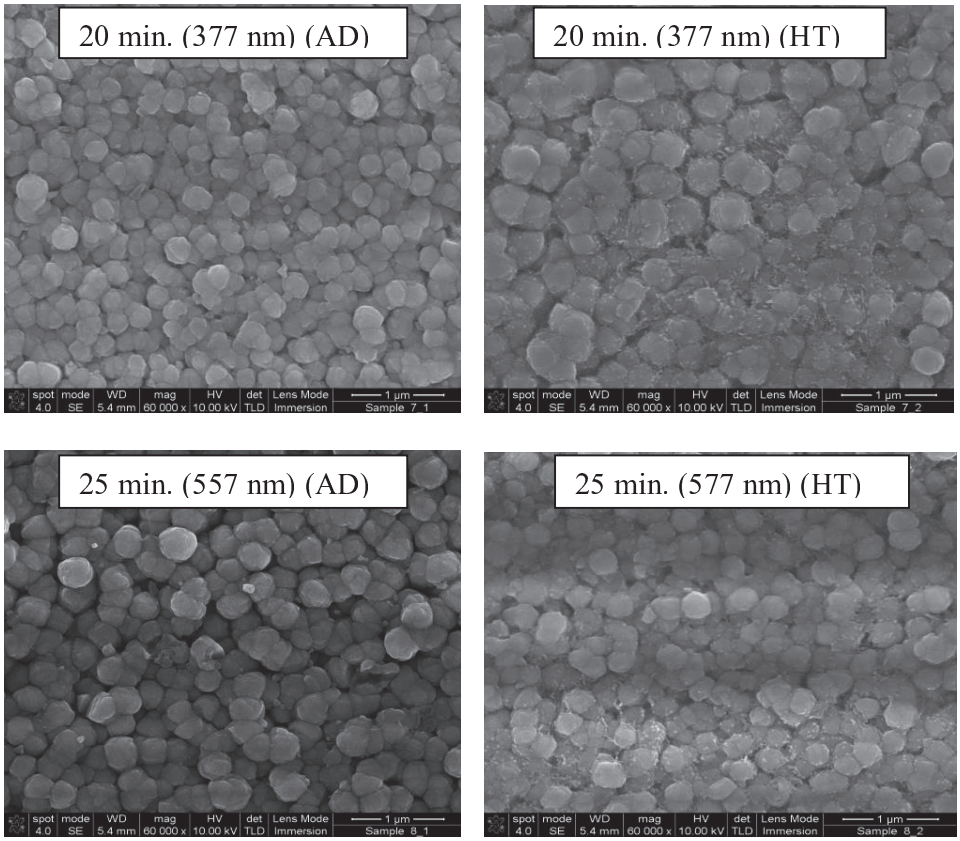

Fig13.xlxs

Fig.14

Click here to download Figure Fig14.doc

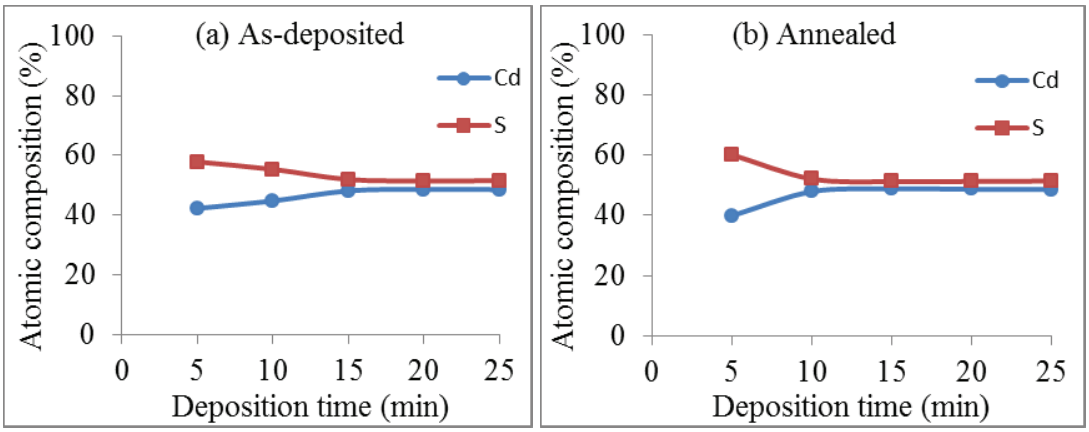

Fig14.xlxs